Dalton Transactions

Altering the solubility of metal-organic polyhedra via pendant functionalization of $Cp_3Zr_3O(OH)_3$ nodes

Journal:	*Dalton Transactions*
Manuscript ID	DT-ART-10-2022-003401.R1
Article Type:	Paper
Date Submitted by the Author:	06-Dec-2022
Complete List of Authors:	Sullivan, Meghan; University at Buffalo, Chemistry Sokolow, Gregory; University at Buffalo, Chemistry Jensen, Eric; University at Buffalo, Chemistry Crawley, Matthew; University at Buffalo, Chemistry MacMillan, Samantha; Cornell University, Chemistry and Chemical Biology Cook, Timothy; University at Buffalo, Chemistry

ARTICLE

Altering the solubility of metal-organic polyhedra via pendant functionalization of $Cp_3Zr_3O(OH)_3$ nodes

Received 00th January 20xx,
Accepted 00th January 20xx

DOI: 10.1039/x0xx00000x

Meghan G. Sullivan, [a] Gregory E. Sokolow, [a] Eric T. Jensen,[b] Matthew R. Crawley,[a] Samantha N. MacMillan,[c] and Timothy R. Cook*[a]

The chemistry of zirconium-based metal-organic polyhedra (ZrMOPs) is often limited by their poor solubulities. Despite their attractive features—including high yielding and facile syntheses, predictable topologies, high stability, and tunability—problematic solubilities have caused ZrMOPs to be under-studied and under-applied. Although these cages have been synthesized with a wide variety of carboxylate-based bridging ligands, we explored a new method for ZrMOP functionalization via node-modification, which we hypothesized could influence solubility. Herein, we report ZrMOPs with benzyl-, vinylbenzyl-, and trifluoromethylbenzyl-pendant groups decorating cyclopentadienyl moieties. The series was characterized by $^1H/^{19}F$ NMR, high-resolution mass spectrometry, infrared spectroscopy, and single-crystal X-ray diffraction. The effects of node functionalities on ZrMOP solubility were quantified using inductively coupled plasma mass spectrometry. Subsitution caused a decreased in water solubility, but for certain organic solvents, e.g. DMF, solubility could be enhanced by ~20x, from 16 μM for the unfunctionalized cage to 310 μM for the vinylbenzyl- and trifluoromethylbenzyl- cages.

Introduction

Metal-organic polyhedra (MOPs) are molecular compounds that are often formed via self-assembly reactions.[1] These permanently porous materials share structural features with metal-organic frameworks (MOFs).[2] In fact, certain MOPs reproduce the topology of individual MOF pores with high fidelity.[3] For example, the cuboctahedral pores of HKUST-1, containing Cu paddlewheel nodes, are reproduced in Cu-MOP.[4, 5] Likewise the pores in UiO-66 are reproduced in ZrMOPs.[6, 7] Part of the motivation for reducing MOFs to these singular cavities is the hypothesis that their molecular nature will improve their solution-phase processability and enable incorporation into hybrid organic/inorganic materials.[8] Depending on solvents and counterions, certain MOPs are poorly soluble, which introduces challenges in fabricating well dispersed hybrid materials for separations,[9-13] guest capture,[14] biomedicine,[15] and catalysis.[16, 17]

We have been particularly interested in zirconium-based metal-organic polyhedra (ZrMOPs) that are synthesized analogously to UiO-66.[6, 18] ZrMOPs have shown promise for applications such as gas separation, small molecule capture, and catalysis.[19-21] These cages comprise six-coordinate, trinuclear zirconium nodes (half that of the UiO-66 cluster) with three cyclopentadiene capping ligands and carboxylate-based bridging ligands.[18] ZrMOPs with 180° bridging ligands generally form tetrahedral (V_4L_6) architectures as a kinetic product, and lantern (V_2L_3) architectures as a thermodynamic product, though ligand geometry also plays a role.[19, 22]

The most common route to solubilization of ZrMOPs is counterion exchange.[23] The use of zirconocene dichloride as a precursor delivers ZrMOPs with chloride counterions, which can be exchanged post-synthetically with triflates to enhance solubility. These counterion exchange reactions are shown to affect the tetrahedra vs lantern distribution via host/guest chemistry.[22] These structural changes may be undesirable for applications where the ZrMOP structure is integral to function. The insolubility of ZrMOPs can also be mitigated through bridging ligand functionalization, but modification of this component also affects pore size and cavity shape.[23, 24]

ZrMOPs contain cyclopentadienyl ligands at the $Cp_3Zr_3O(OH)_3$ nodes. Examples of functionalizing these capping ligands are rare. In fact, only *n*-butyl pendants have been reported thus far.[19, 25] We hypothesized that the cyclopentadienyl ligands could be used as general sites for functionalization to tune the properties of such MOPs. This approach has an advantage in that it doesn't change the organic bridging ligands so that the overall topology and self-assembly should be invariant to the modifications. For these studies, **ZrMOP** with a 1,4-benzenedicarboxylate ligand was used as the core structure. Three new MOPs were then synthesized with node-based benzyl-, vinylbenzyl-, and trifluoromethylbenzyl-moieties, named **ZrMOP-ben**, **ZrMOP-vb**, and **ZrMOP-tfmb**, respectively. These ZrMOPs were fully characterized through $^1H/^{19}F$ NMR, high-resolution mass spectrometry, infrared

[a] *Department of Chemistry, University at Buffalo, The State University of New York, Buffalo, New York 14260, United States.*
[b] *Chemistry Instrument Center, Department of Chemistry, University at Buffalo, State University of New York, Buffalo, NY 14260, United States.*
[c] *Department of Chemistry and Chemical Biology, Cornell University, Ithaca, New York 14853, United States.*

† Electronic Supplementary Information (ESI) available: Experimental details, NMR spectroscopy, mass spectrometry, infrared spectroscopy, X-ray crystallography, and solubility studies. See DOI: 10.1039/x0xx00000x

spectroscopy, and single-crystal X-ray diffraction. Subsequently, ICP-mass spectrometry was used to evaluate the effects of ZrMOP node-functionality on solubility.

Experimental

Materials

Benzyl bromide and zirconium (IV) tetrachloride were purchased from Alfa Aesar. Dicyclopentadiene and 4-vinylbenzyl chloride were purchased Sigma Aldrich. 4-(trifluoromethyl)benzyl chloride and tetrabutylammonium iodide (TBAI) were purchased from Oakwood Chemical. Zirconocene dichloride (Cp_2ZrCl_2) was purchased from Strem Chemicals. *n*-butyllithium 1.6 M in hexanes was purchased from Acros Organics. 1,4-benzenedicarboxylic acid (terephthalic acid) was purchased from TCI. Dry solvents (THF, toluene, hexanes, diethyl ether) were purified using a solvent drying system (Pure Process Technology).

Methods

^{1}H and ^{19}F{^{1}H} nuclear magnetic resonance (NMR) spectra were acquired in 32-128 scans using a Bruker AVANCE NEO 500 spectrometer. Chemical shifts (δ) are reported in parts per million (ppm) referenced using the residual proton solvent peaks. Multiplicities are indicated as singlets (s), doublets (d), triplets (t) or multiplets (m). All mass spectrometry samples were prepared in methanol. High-resolution mass spectrometry (HRMS) experiments for **ZrMOP** and **ZrMOP-ben** were completed using electrospray ionization (ESI) on a 12 T Bruker SolariX FT-ICR-MS. A Thermo Fisher Q-Exactive Liquid Chromatograph Orbitrap Tandem Mass Spectrometer was used for ESI-HRMS of **ZrMOP-vb** and **ZrMOP-tfmb**. Fourier transform infrared (FTIR) spectra were acquired with a PerkinElmer 1760 FTIR spectrometer with horizontal attenuated total reflectance (ATR) on neat ZrMOP powders.

Synthesis of Sodium Cyclopentadiene (NaCp). Synthesis was carried out following a modified literature procedure.[26] Synthesis, work-up, and storage were performed in either a moisture-free argon or nitrogen atmosphere, with dry solvents. Dicyclopentadiene was freeze-pump-thawed in triplicate and subsequently distilled under argon at 170°C (distillate at 41°C) into a receiving flask cooled to −78°C. Sodium metal (6.7 g, 290 mmol) was shaved into small pieces, rinsed well with toluene, and added to a 200 mL Schlenk flask with THF (40 mL). After the flask was cooled to −78°C, the freshly distilled cyclopentadiene monomer (25 mL) was cannula transferred dropwise into the sodium metal suspension. The reaction was stirred at –78°C for three hours before it was slowly warmed to room temperature. After 24 hours, the pink solution was cannula transferred in to a new Schlenk flask, leaving behind unreacted sodium metal. Dynamic vacuum was used to remove THF, yielding a faint pink solid. The solid was loaded onto a fine fritted glass funnel and washed three times with hexanes. The white solid was dried under dynamic vacuum at 60°C for 24 hours. The NaCp was dissolved in THF (82 mL) to make a 2.4 M solution and was stored under nitrogen. Yield = 18 g (61%). ^{1}H NMR (500 MHz, DMSO-d_6, 25°C): δ (ppm) = 5.35 (s, Cp).

(p-benzyl)cyclopentadiene. Synthesis and work-up were carried out following a modified literature procedure.[27] The synthesis was performed in a moisture-free argon atmosphere, with dry solvents. *p*-benzyl bromide (2.7 mL, 23 mmol) was dissolved in ~90 mL of THF and cooled to 0°C. 13 mL (31 mmol) of a 2.4 M solution of NaCp in THF was diluted with an additional 21 mL of THF and subsequently cannula transferred dropwise into the *p*-benzyl bromide solution. The solution turned yellow, followed by the appearance of an off-white precipitate. After 10 minutes, TBAI (17 mg, 0.20 mol %) was added and allowed to stir for an additional 10 minutes. The suspension was warmed to room temperature and stirred for 13 hours. The pale-yellow suspension was quenched with brine, neutralized with 0.1 M HCl, and the organic layer extracted and washed two times with brine. After stirring the yellow solution over magnesium sulfate for 1 hour, THF was removed under dynamic vacuum at 40°C to yield an orange oil. The product was purified by gravity-mediated column chromatography on a 6-inch tall, 1.5-inch diameter silica column in 2% ethyl acetate/hexanes (R_f = 0.4). The product was isolated as a mixture of two isomers as a clear colourless liquid. The material was used in subsequent reactions within 12 hours. Yield = 1.6 g (44%). ^{1}H NMR (500 MHz, $CDCl_3$, 25°C): δ (ppm) = 7.30 (m, benzyl CH, 2H), 7.21 (m, benzyl CH, 3H) 6.42 (m, Cp CH, 1.6 H), 6.29 (m, Cp CH, 0.4H), 6.18 (m, Cp CH, 0.4H), 6.02 (m, Cp CH, 0.6H), 3.75 (s, CH_2, 0.8H), 3.72 (s, CH_2, 1.2H), 3.00 (m, Cp CH_2, 1.2H), 2.87 (m, Cp CH_2, 0.8H).

(p-vinylbenzyl)cyclopentadiene. Synthesis and work-up were carried out following a modified literature procedure.[28] The synthesis was performed in a moisture-free argon atmosphere, with dry solvents. *p*-vinylbenzyl chloride (2.3 mL, 16 mmol) was dissolved in ~60 mL of THF and cooled to 0°C. 9.2 mL (22 mmol) of a 2.4 M solution of NaCp in THF was diluted with an additional 17 mL of THF and subsequently cannula transferred dropwise into the *p*-vinylbenzyl chloride solution. The solution turned bright yellow, and later into a light-brown suspension. After 10 minutes, TBAI (12 mg, 0.20 mol %) was added and allowed to stir for an additional 10 minutes. The suspension was warmed to room temperature and stirred for 13 hours. The light-brown suspension was quenched with water, neutralized with 0.1 M HCl, and the organic layer extracted and washed two times with brine. After stirring the yellow solution over magnesium sulfate for 1 hour, THF was removed under dynamic vacuum at 40°C to yield an orange oil. The product was purified by gravity mediated column chromatography on a 6-inch tall, 1.5-inch diameter silica column in 100% hexanes (R_f = 0.2). The product was isolated as a mixture of two isomers as a clear colourless liquid. The material was used in subsequent reactions within 12 hours. Yield = 1.2 g (40%). ^{1}H NMR (500 MHz, $CDCl_3$, 25°C): δ (ppm) = 7.33 (dd, aromatic CH, 2H), 7.16 (dd, aromatic CH, 2H)

6.70 (dd, vinyl CH, 1H) 6.42 (m, Cp CH, 1.5H), 6.28 (m, Cp CH, 0.5H), 6.17 (m, Cp CH, 0.5H), 6.01 (m, Cp CH, 0.5H), 5.71 (dd, vinyl CH_{trans}, 1H), 5.20 (dd, vinyl CH_{cis}, 1H), 3.73 (s, CH_2, 0.9H), 3.70 (s, CH_2, 1.1H), 2.99 (m, Cp CH_2, 1.1H), 2.86 (m, Cp CH_2, 0.9H).

(p-trifluoromethylbenzyl)cyclopentadiene. The synthesis was performed in a moisture-free argon atmosphere, with dry solvents. *p*-triflororomethylbenzyl chloride (3.0 mL, 21 mmol) was dissolved in ~80 mL of THF and cooled to 0°C. 12 mL (28 mmol) of a 2.4 M solution of NaCp in THF was diluted with an additional 21 mL of THF and subsequently cannula transferred dropwise into the *p*-trifluoromethylbenzyl chloride solution. The solution became a light-brown suspension. After 10 minutes, TBAI (15 mg, 0.20 mol %) was added and allowed to stir for an additional 10 minutes. The suspension was warmed to room temperature and stirred for 13 hours. The brown suspension was quenched with water, neutralized with 0.1 M HCl, and the organic layer extracted and washed two times with brine. After stirring the yellow solution over magnesium sulfate for 1 hour, THF was removed under dynamic vacuum at 40°C to yield an orange oil. The product was purified by gravity-mediated column chromatography on a 6-inch tall, 1.5-inch diameter silica column in 3% ethyl acetate/hexanes (R_f = 0.5). The product was isolated as a mixture of two isomers as a clear colourless liquid. The material was used in subsequent reactions within 12 hours. Yield = 920 mg (20%). ^{1}H NMR (500 MHz, $CDCl_3$, 25°C): δ (ppm) = 7.54 (d, aromatic CH, 2H), 7.31 (t, aromatic CH, 2H), 6.47 – 6.41 (m, Cp CH, 1H), 6.39 – 3.36 (m, Cp CH, 0.6H), 6.30 (m, Cp CH, 0.4H), 6.17 (p, Cp CH, 0.4H), 6.03 (p, Cp CH, 0.6H), 3.80 (s, CH_2, 0.8H), 3.76 (s, CH_2, 1.2H), 3.00 (m, Cp CH_2, 1.2H), 2.86 (m, Cp CH_2, 0.8H). ^{19}F{^{1}H} NMR (470 MHz, ($CDCl_3$, 25 °C): δ (ppm) = −63.51 (s, CF_3).

(p-benzylcyclopentadiene)zirconium dichloride. The synthesis and work-up were carried out following a modified literature procedure,[29] in a moisture-free nitrogen atmosphere, with dry solvents. In a 200 mL flask, (*p*-benzyl)cyclopentadiene (992 mg, 6.35 mmol) was added to diethyl ether (60 mL) and cooled in a liquid nitrogen trap for 10 minutes. *n*-BuLi (2.5 M, 2.54 mL, 6.35 mmol) was then added dropwise to the stirring solution, yielding a bright yellow solution and then a thick, cream-colored suspension. The suspension was cooled for another 5 minutes before zirconium tetrachloride (740 mg, 3.17 mmol) was transferred into the flask. The suspension was warmed to room temperature and stirred for 20 hours. The pale-yellow suspension was then filtered through a fine fritted glass funnel, and the solid washed twice with excess diethyl ether. The solvent was removed from the filtrate until ~10 mL of solvent remained. The resulting mixture was filtered through a fine fritted glass funnel and the solid washed with hexanes three times. The solid was dried under a stream of dry nitrogen for 12 hours. Yield = 460 mg (31%). ^{1}H NMR (500 MHz, $CDCl_3$, 25°C): δ (ppm) = 7.30 (t, aromatic CH, 4H), 7.21 (m, aromatic CH, 6H), 6.21 (m, Cp, 8H), 4.01 (s, CH_2, 4H).

(p-vinylbenzylcyclopentadiene)zirconium dichloride. Synthesis and work-up were performed in a moisture-free nitrogen atmosphere, with dry solvents. In a 200 mL flask, (*p*-vinylbenzyl)cyclopentadiene (1.174 g, 6.439 mmol) was added to diethyl ether (60 mL) and cooled in a liquid nitrogen trap for 10 minutes. *n*-BuLi (2.5 M, 2.58 mL, 6.44 mmol) was then added dropwise to the stirring solution yielding a yellow solution and then a thick, cream-colored suspension. The suspension was cooled for another 5 minutes before zirconium tetrachloride (720 mg, 3.09 mmol) was transferred into the flask. The suspension was warmed to room temperature and stirred for 20 hours. The white suspension was then filtered through a fine fritted glass funnel, and the solid washed twice with excess diethyl ether. The solvent removed from the filtrate until ~5 mL of solvent remained. The resulting mixture was filtered through a fine fritted glass funnel and the solid washed with hexanes three times. The solid was dried under a stream of dry nitrogen for 12 hours. Yield = 340 mg (21%). ^{1}H NMR (500 MHz, $CDCl_3$, 25°C): δ (ppm) = 7.34 (d, aromatic CH, 4H), 7.16 (d, aromatic CH, 4H), 6.69 (dd, vinyl CH, 2H), 6.22 (dt, Cp, 8H), 5.71 (d, vinyl CH_{trans}, 2H), 5.21 (d, vinyl CH_{cis}, 2H), 4.00 (s, CH_2, 4H).

(p-trifluoromethylbenzylcyclopentadiene)zirconium dichloride. Synthesis and work-up were performed in a moisture-free nitrogen atmosphere, with dry solvents. In a 100 mL flask, (*p*-trifluoromethylbenzyl)cyclopentadiene (907 mg, 4.05 mmol) was added to diethyl ether (40 mL) and cooled in a liquid nitrogen trap for 10 minutes. *n*-BuLi (2.5 M, 1.62 mL, 4.05 mmol) was added dropwise to the stirring solution yielding a thick cream-colored suspension. The suspension was cooled for another 5 minutes before zirconium tetrachloride (452 mg, 1.94 mmol) was transferred into the flask. The suspension was warmed to room temperature and was stirred for 20 hours. The yellow suspension was then filtered through a fine fritted glass funnel and the solid washed twice with excess diethyl ether. The solvent was removed from the filtrate until ~3 mL of solvent remained. This solvent was decanted and discarded. The solid was then washed with hexanes and immediately decanted three times. The solid was dried under a stream of dry nitrogen for 12 hours. Yield = 510 mg (43%). ^{1}H NMR (500 MHz, $CDCl_3$, 25°C): δ (ppm) = 7.55 (d, aromatic CH, 4H), 7.32 (d, aromatic CH, 4H), 6.26 (dt, Cp, 8H), 4.10 (s, CH_2, 4H).

ZrMOP. In a 250 mL flask, zirconocene dichloride (200 mg, 0.68 mmol, 1.0 eq.) and 1,4-benzenedicarboxylic acid (57 mg, 0.34 mmol, 0.50 eq.) were combined, followed by a 5:1 DMF (5.7 mL) to H_2O (1.1 mL) mixture. The reaction mixture was sonicated for 30 seconds and was subsequently left undisturbed at room temperature for 20 hours. The colourless reaction solution was then decanted from the white precipitate. The precipitate was washed and decanted once with fresh DMF, and three times with chloroform by centrifugation. Solvent was removed under reduced pressure at 60°C for 6 hours to give product as a white solid. Yield = 140 mg (76%). ^{1}H NMR (500 MHz, DMSO-d_6, 25°C): δ (ppm) = 10.61 (s, μ-OH, 12H), 7.95 (s, bdc CH, 24H), 6.64 (s, Cp, 60H). FT-ICR-MS, [M]= $C_{108}H_{96}O_{40}Zr_{12}Cl_4$, experimental (calc., error) m/z: 781.85030 (781.85304, –3.50 ppm) $[M–4Cl^–]^{4+}$, 1042.12967 (1042.13496, –5.07 ppm) $[M–4Cl^––H^+]^{3+}$, 1562.68584 (1562.69880, –8.29 ppm) $[M–4Cl^––2H^+]^{2+}$, 2095.89822 (2095.92160, –11.15 ppm) $[2M–7Cl^––4H^+]^{3+}$. FTIR (ν, $cm^{–1}$): 3133, 1652, 1547, 1504, 1404, 1016, 810, 745, 601, 549.

ZrMOP-ben. In a 2-dram vial, (*p*-benzylcyclopentadiene)zirconium dichloride (150 mg, 0.32 mmol, 1.0 eq.) and 1,4-benzenedicarboxylic acid (26 mg, 0.16 mmol, 0.50 eq.) were combined, followed by a 5:1 DMF (6.7 mL) to H_2O (0.5 mL) mixture. The reaction mixture was sonicated for 30 seconds and was subsequently left undisturbed at room temperature for 20 hours. The pale-yellow reaction solution was then decanted from the white precipitate. The precipitate was washed and decanted once with fresh DMF, and three times with chloroform by centrifugation. Solvent was removed under reduced pressure at 60°C for 6 hours to give product as a white solid. Yield = 86 mg (74%). ^{1}H NMR (500 MHz, DMSO-d_6, 25°C): δ (ppm) = 10.50 (s, μ-OH, 12H), 8.13 (s, bdc CH, 24H), 7.23—7.11 (m, aromatic CH, 60H), 6.58 (s, Cp, 48H), 4.00 (s, CH_2, 24H). FT-ICR-MS, [M]= $C_{192}H_{168}O_{40}Zr_{12}Cl_4$, experimental (calc., error) m/z: 1052.24614 (1052.24467, 1.40 ppm) $[M–4Cl^–]^{4+}$, 1402.65864 (1402.65713, 1.08 ppm) $[M–4Cl^––H^+]^{3+}$, 2103.48021 (2103.48205, –0.87 ppm) $[M–4Cl–2H^+]^{2+}$. FTIR (ν, $cm^{–1}$): 3082, 1657, 1557, 1505, 1393, 813, 745, 702, 611, 547.

ZrMOP-vb. In a 2-dram vial, (*p*-vinylbenzylcyclopentadiene)zirconium dichloride (100 mg, 0.19 mmol, 1.0 eq.) and 1,4-benzenedicarboxylic acid (16 mg, 0.095 mmol, 0.50 eq.) were combined, followed by a 5:1 DMF (1.6 mL) to H_2O (0.3 mL) mixture. The reaction mixture was sonicated for 30 seconds and was subsequently left undisturbed at room temperature for 20 hours. The pale-yellow reaction solution was decanted from the white precipitate. The precipitate was washed and decanted once with fresh DMF, and three times with chloroform by centrifugation. Solvent was removed under reduced pressure at 60°C for 6 hours to give product as a white solid. Yield = 55 mg (74%). ^{1}H NMR (500 MHz, DMSO-d_6, 25°C): δ (ppm) = 10.58 (s, μ-OH, 11H), 8.11 (s, bdc CH, 24H), 7.27 (d, aromatic CH, 24H), 7.18 (d, aromatic CH, 24H), 6.62 (m, Cp and vinyl CH overlapped, 60H), 5.71 (d, vinyl CH_{trans}, 12H), 5.19 (d, vinyl CH_{cis}, 12H), 4.00 (s, CH_2, 24H). Q-Exactive Orbitrap-MS, [M]= $C_{216}H_{192}O_{40}Zr_{12}Cl_4$, experimental (calc., error) m/z: 1130.2899 (1130.2918, –1.68 ppm) $[M–4Cl^–]^{4+}$, 1506.7174 (1506.7200, –1.73 ppm) $[M–4Cl^––H^+]^{3+}$, 2259.5744 (2259.5763, –0.84 ppm) $[M–4Cl^––2H^+]^{2+}$. FTIR (ν, $cm^{–1}$): 3000, 1655, 1557, 1504, 1388, 820, 744, 611, 548.

ZrMOP-tfmb. In a 2-dram vial, (*p*-trifluoromethylbenzylcyclopentadiene)zirconium dichloride (200 mg, 0.33 mmol, 1.0 eq.) and 1,4-benzenedicarboxylic acid (27 mg, 0.16 mmol, 0.50 eq.) were combined, followed by a 5:1 DMF (2.7 mL) to H_2O (0.6 mL) mixture. The reaction mixture was sonicated for 30 seconds and was subsequently left undisturbed at room temperature for 20 hours. The colourless reaction solution was then decanted from the white precipitate. The precipitate was washed and decanted once with fresh DMF, and three times with chloroform by centrifugation. Solvent was removed under reduced pressure at 60°C for 6 hours to give product as a white solid. Yield = 95 mg (67%). ^{1}H NMR (500 MHz, DMSO-d_6, 25°C): δ (ppm) = 10.61 (s, μ-OH, 12H), 8.10 (s, bdc CH, 24H), 7.53 (d, aromatic CH, 24H), 7.43 (d, aromatic CH, 24H), 6.62 (s, Cp, 48H), 4.10 (s, CH_2, 24H). ^{19}F{^{1}H} NMR (470 MHz, DMSO-d_6, 25 °C): δ (ppm) = v61.64 (s, CF_3). Q-Exactive Orbitrap-MS, [M]= $C_{204}H_{156}O_{40}Zr_{12}F_{36}Cl_4$, experimental (calc., error) m/z: 1256.2044 (1256.2069, –1.99 ppm) $[M–4Cl^–]^{4+}$, 1674.6030 (1674.6068, –2.27 ppm) $[M–4Cl^––H^+]^{3+}$, 2511.4030 (2511.4066, –1.43 ppm) $[M–4Cl^––2H^+]^{2+}$. FTIR (ν, $cm^{–1}$): 3077, 1577, 1506, 1394, 1322, 1160, 1118, 1107, 1066, 1018, 814, 744, 612, 548.

Single ZrMOP Crystals

Crystals for single crystal X-ray diffraction (SC-XRD) studies were collected directly out of reaction mixtures. For optimal crystal quality, synthetic conditions were slightly modified. The zirconocene precursor (1.0 eq., 50 mg) was combined with 1,4-benzenedicarboxylic acid (0.50 eq.). The reactants were sonicated in DMF until completely dissolved. The solution was then filtered through a microfiber pipette filter into a new 1-dram vial. A 1:1 mixture of DMF:H_2O was made, using the amount of H_2O specified in the usual ZrMOP synthesis. This solution was added dropwise to the solution of reactants in DMF, with gentle shaking between drops. The clear solutions were capped and allowed to sit undisturbed at room temperature until crystals formed. Tetrahedral architectures were observed by SC-XRD from crystals collected within 1 week, and lantern architectures were collected with longer reaction times.

ICP-MS Sample Preparation

Methods, materials, and detailed experimental procedures for ICP-MS studies can be found in the supplementary information (page S34). ICP-MS samples were made in triplicate for each ZrMOP per solvent, using three independently synthesized batches of ZrMOP. Saturated solutions of each ZrMOP were made in dimethylformamide, dimethyl sulfoxide, methanol, and water by stirring ZrMOP suspensions in 2 mL of solvent for 1 hour at room temperature, followed by filtration through packed celite. 100 μL of each solution was added to 1 mL of nitric acid and heated at 60°C for 3 days to digest the ZrMOP. After 3 days, the solutions were cooled to room temperature and diluted to 25 mL with nano-pure water. Further dilutions with 2.5% nitric acid were performed to attain concentrations suitable for ICP-MS.

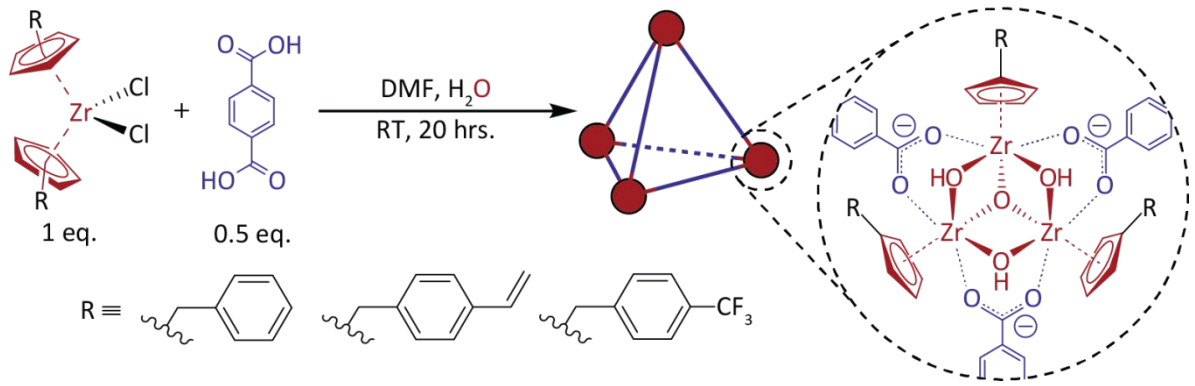

Figure 1. Synthesis of functionalized ZrMOPs.

Results & Discussion

Starting materials for ZrMOP self-assembly reactions were prepared following Scheme 1. The functionalized cyclopentadiene precursors are prone to degradation as evidenced by ^{1}H NMR (Figure S6), so they were used in subsequent reactions within 12 hours of purification. Functionalized zirconocenes sublimed under dynamic vacuum at room temperature, thus they were dried under inert gas flow for approximately 12 hours.

ZrMOPs form tetrahedral architectures (V_4L_6) under kinetic control, and lantern architectures (V_2L_3) with thermodynamic control.[22, 23] Many classic ZrMOP self-assembly conditions result in a mixture of the two architectures. For example, the synthesis of **ZrMOP** at 60°C for 20 hours results in roughly a 50:50 mixture of the two topologies, as evidenced by ^{1}H NMR (Figure S16) and mass spectrometry (Figure S21). To isolate a pure tetrahedral phase, our ZrMOP assembly reactions were carried out at room temperature for 20 hours (Figure 1). Despite the lower reaction temperature, ZrMOPs were still isolated in good yields (66-76%).

Scheme 1

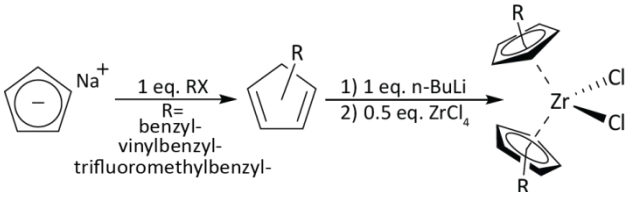

^{1}H NMR of the parent **ZrMOP** shows a single μ-OH peak at 10.61 ppm, which appears in the analogous functionalized ZrMOPs between 10.50 and 10.61 ppm (Figure 2). The lantern architectures exhibit a distinct μ-OH peaks slightly upfield of the tetrahedron μ-OH resonances and in mixtures of the two, both peaks are well resolved (example shown in Figure S16). We attribute singular peaks to be indicative of pure tetrahedral phases.

The spectrum of **ZrMOP** has a peak at 7.95 ppm due to the 24 equivalent protons of the bridging ligand. Because this resonance overlaps with the aldehyde proton of DMF, it integrates slightly higher than 24 protons, but can be corrected for DMF content using the -CH_3 resonances of DMF at 2.89 or 2.73 ppm. In the functionalized ZrMOPs, the bridging ligand is comparatively deshielded, and appears between 8.10 and 8.13 ppm. The presence of single aromatic resonances from 1,4-bdc also support pure tetrahedral MOP phases, as the lantern/tetrahedron mixtures have second 1,4-bdc peaks shifted upfield (example shown in Figure S16).

The spectrum of **ZrMOP** has a singlet at 6.64 ppm ascribed to the 60 cyclopentadienyl protons, and the analogous signal in the functionalized ZrMOPs appears between 6.58 and 6.62 ppm and integrates to 48 protons, as expected. Notably for **ZrMOP-vb**, the cyclopentadienyl resonance overlaps with a vinyl proton resonance. These cyclopentadienyl resonances are sharp, which again supports the pure tetrahedral phase in solution, as the cyclopentadienyl resonance broadens when there is a mixture of both lantern and tetrahedral architectures (example shown in Figure S16).

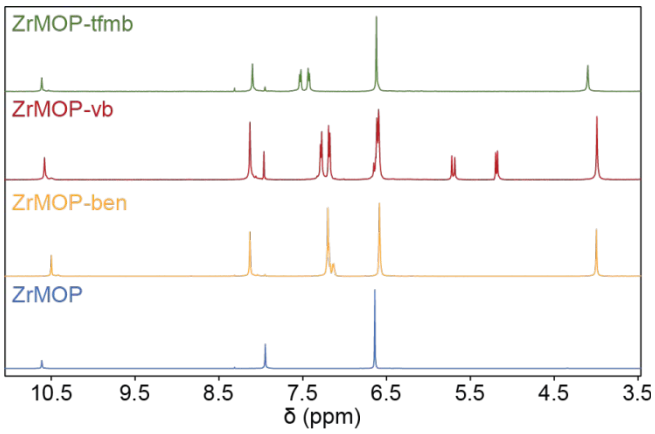

Figure 2. Stacked ^{1}H NMR spectra of **ZrMOP** and functionalized analogues, in DMSO-d_6 at room temperature.

The benzyl protons of **ZrMOP-ben** appear between 7.11 and 7.23 ppm, whereas **ZrMOP-vb** benzyl protons are deshielded to 7.18 and 7.27 ppm, and **ZrMOP-tfmb** benzyl protons are further deshielded with resonances at 7.43 and 7.53 ppm. The methylene linker protons of the benzyl group appear at 4.00 ppm in the cases of **ZrMOP-ben** and **ZrMOP-vb** but are

shifted downfield to 4.10 ppm in the spectrum of **ZrMOP-tfmb**. **ZrMOP-tfmb** also has a single ^{19}F resonance at −61.64 ppm due to the twelve equivalent CF_3 groups. μ-OH, aromatic, and cyclopentadienyl ^1H NMR resonances all support that the functionalized ZrMOPs were isolated as tetrahedra.

High resolution mass spectrometry confirmed the presence of intact V_4L_6 ZrMOPs (Figure 3) containing four vertices and six bridging carboxylates. The same charge states were observed for all of the cages studied, with 3+ base peaks corresponding to [M]−4Cl⁻−H⁺. The 2+ ([M]−4Cl⁻−2H⁺) and 4+ ([M]−4Cl⁻) peaks in these mass spectra display unique isotope patterns for the lantern (V_2L_3) and tetrahedral (V_4L_6) ZrMOPs. This allows for a qualitative assessment of which architectures are present in the samples.

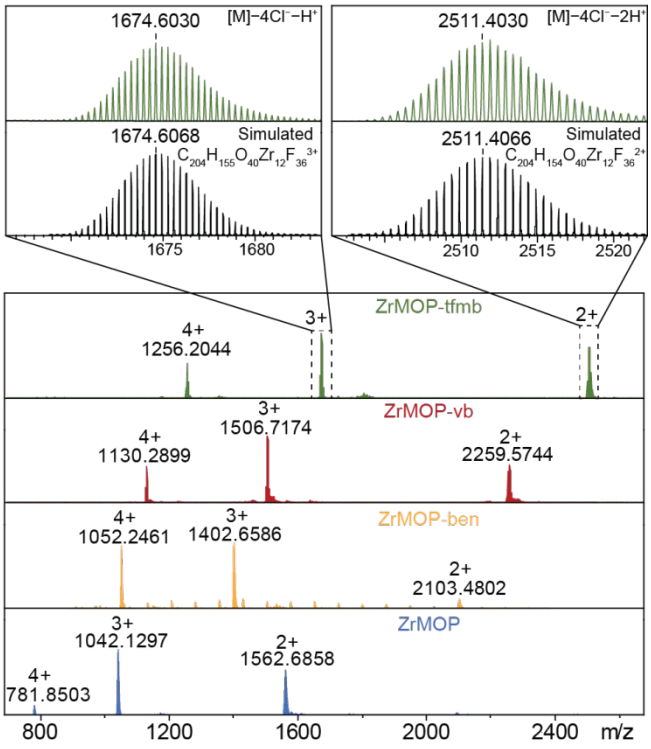

Figure 3. Stacked high resolution mass spectra of **ZrMOP** and functionalized analogues, with simulated and experimental isotope patterns of **ZrMOP-tfmb** 2+ and 3+ charge states.

For example, Figure S21 shows that higher reaction temperatures yield a mixture of the two **ZrMOP** architectures. Each lantern architecture is half of the mass, and half of the charge of the corresponding tetrahedron. Thus, the m/z value for the 1+ peak of V_2L_3 **ZrMOP** is shared with the 2+ peak of V_4L_6 **ZrMOP.** The same is true for the 2+ and 4+ peaks of the lantern and tetrahedral **ZrMOP**. The experimental isotope pattern does not match the predicted 1+ peak of a **ZrMOP** lantern, or the predicted 2+ peak of a **ZrMOP** tetrahedron. Instead, an overlay of both is observed. Previous literature studies on ZrMOPs have seen a similar overlay of charge states.[22] This indicates that the **ZrMOP** is present as a mixture of both architectures under these synthetic conditions.

Under kinetic control, there is agreement between the experimental 2+ isotope pattern and the simulated 2+ pattern of the tetrahedral **ZrMOP** ([M]−4Cl⁻−2H⁺). There is no apparent contribution from a 1+ peak of lantern architecture ([M]−2Cl⁻−H⁺), shown in Figure S17. High-resolution mass spectrometry data of all ZrMOPs shows agreement with the predicted isotope patterns of tetrahedra, without any apparent contribution from lantern architectures (Figure 3 and Figures S17-S20). Thus, synthesis of these ZrMOPs at room temperature yields the tetrahedral architectures.

Infrared spectra were consistent with literature reports of **ZrMOP** (Figure S22).[30] Minimal residual dimethylformamide was observed in the samples. There are no significant differences between the spectra of **ZrMOP-ben** and **ZrMOP-vb** when compared to **ZrMOP**. That said, **ZrMOP-tfmb** showed several new infrared stretches that can be attributed to the CF_3 group, including peaks at 1322, 1160, 1118, 1107, 1066, and 1018 cm^{-1}.

Evidence of both the tetrahedral and lantern ZrMOPs can be seen directly through SC-XRD, shown in Figure 4. When crystals were collected from reaction mixtures within one week, tetrahedra (the kinetic product) were observed. A suitable dataset for structural analysis was collected for the **ZrMOP-ben** tetrahedron. The **ZrMOP-vb** and **ZrMOP-tmfb** tetrahedra data sets were only suitable to evaluate connectivity. Single crystals of lantern architectures (the thermodynamic product) were isolated for **ZrMOP-ben** and **ZrMOP-tfmb** when the reaction mixture was left undisturbed for approximately a month. No **ZrMOP-vb** crystals were obtained for the lantern architecture despite multiple crystallization attempts.

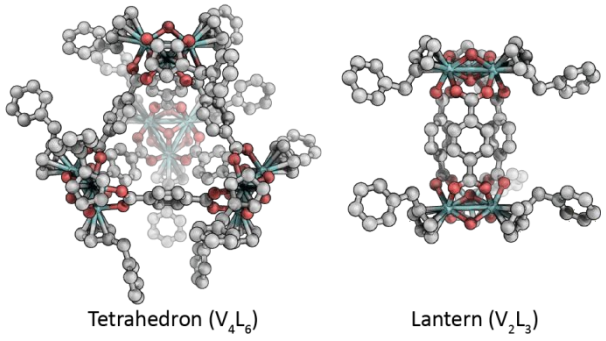

Figure 4. Crystal structures of **ZrMOP-ben** tetrahedron and lantern architectures.

The Zr-hydroxo-Zr angle, Zr-oxo-Zr angle, and the intranodal Zr-Zr metal separation distance of the **ZrMOP-ben** tetrahedron (107.8°, 103.8°, and 3.34 Å, respectively) are similar to the unfunctionalized **ZrMOP** tetrahedron (107.8°, 103.6°, 3.35 Å), showing that node functionality has minimal effect on the metal-oxide node structure. The Zr-Zr distance along the edge of the tetrahedron is also unaffected, remaining 11.1 Å for both **ZrMOP-ben** and the unfunctionalized **ZrMOP**.[6] Overlays of ZrMOP-ben and the unfunctionalized ZrMOP tetrahedron show no significant geometric changes are imparted by node

functionalization (Figure S23). Thus, part of the benefit of this work is that we can modify the periphery of ZrMOPs without causing any changes to the parent MOP architecture, which is dependent upon the bridging ligand geometry.

The separation distance between zirconium nodes of adjacent MOPs can be assessed by examining the distance between the centroid points of the Zr-Zr-Zr plane within a metal-oxide node (Figure S33). The separation to the nearest adjacent **ZrMOP** is relatively consistent across **ZrMOP-ben** tetrahedron, **ZrMOP-tfmb** lantern, and **ZrMOP-ben** lantern, increasing slightly across the series (7.1, 7.3, and 7.4 Å respectively). This can be attributed to μ_2-OH bridges of the zirconium nodes participating in hydrogen bonding with chloride counterions and solvent molecules (DMF and H_2O) which organizes neighbouring MOPs across the crystal structures (Figure S32). This same hydrogen bond network is observed in the crystal packing of the unfunctionalized **ZrMOP** tetrahedron, which has a separation of 7.1 Å.[6]

In addition to hydrogen bonding, hydrophobic interactions between the functional side chains of the cyclopentadienyl capping ligands are prevalent. This is especially clear in the **ZrMOP-tfmb** lantern packing wherein adjacent cages pack such that trifluoromethylbenzyl- substituents from both MOPs interlock with one another, thereby minimizing side chain-solvent interactions (Figure S30, crystallographic *a* direction). Further analysis of the solid-state packing reveals that **ZrMOP-tfmb** lantern exhibits 4.8 x 8.2 Å channels running along the crystallographic *b* direction (Figure S30). These sorts of organized void spaces are much less apparent in the **ZrMOP-ben** lantern and tetrahedron structures (Figure S29 and Figure S31).

This series of ZrMOPs do not have any UV-vis absorption bands that enable quantification of their concentration in solution. Thus, inductively coupled plasma mass spectrometry was used to quantify zirconium content in saturated solutions of the ZrMOPs, as has been done for other Zr-containing species.[31-33] This was carried out in solvents with a range of dielectric constants and experimental polarity indices (dielectric constant, polarity index), including dimethylformamide (36.7, 0.386), dimethyl sulfoxide (46.7, 0.444), methanol (32.7, 0.762), and water (80.1, 1.00).[34] To account for variability between batches of ZrMOPs, ICP-MS was performed using samples prepared in triplicate from three independently synthesized batches of each ZrMOP. Samples were prepared with corresponding matrix blanks. The average relative standard deviation in solubility across all samples was 17%, and detailed results can be found in Tables S4-S7.

By adding node functionality to **ZrMOP**, all three analogues had approximately a 7-fold decrease in water solubility, with saturation limits dropping from about 10 to 1.5 µM. In methanol there is also a decrease in the solubility of ZrMOPs, with **ZrMOP-ben** and **ZrMOP-tfmb** having less than one-third of the solubility of the unfunctionalized **ZrMOP**. With the addition of twelve hydrophobic benzyl substituents per ZrMOP, these solubility trends are reasonable in polar, protic solvents like water and methanol.

In terms of processability of ZrMOPs, most post-synthetic modifications or materials processing methods require solubility in organic solvents. Thus, enhancing solubility in organics is favourable. Dimethyl sulfoxide is an aprotic, coordinating solvent that is a common NMR solvent for ZrMOPs. **ZrMOP-vb** showed enhanced solubility in DMSO, increasing from a saturation limit of 1.0 mM to 1.5 mM. The solubility of **ZrMOP-ben** was quite unchanged and the solubility of **ZrMOP-tfmb** decreased by about 0.2 mM, relative to **ZrMOP**.

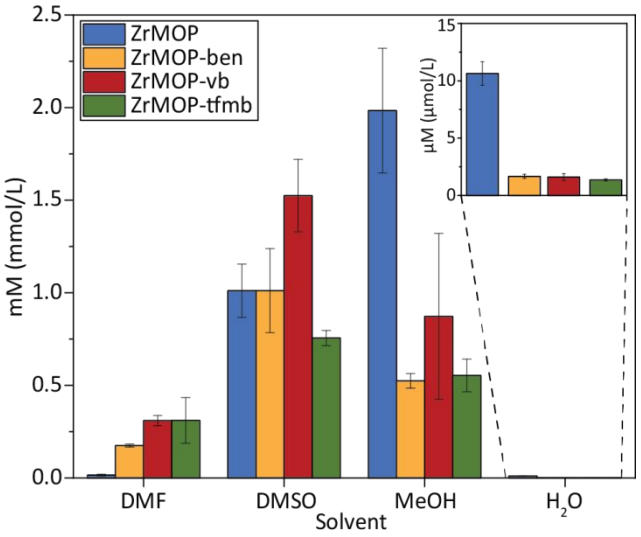

Figure 5. Graphical representation of the solubility of **ZrMOP** and functionalized analogues in dimethylformamide (DMF), dimethyl sulfoxide (DMSO), methanol (MeOH), and water (H_2O).

ZrMOP self-assembly reactions are usually carried out in dimethylformamide, so it is also a relevant organic solvent for these studies. Solubility in DMF proved to be the most tunable through node-functionalization. **ZrMOP** has a solubility of merely 16 µM in DMF, which increased over 10-fold (176 µM) with the benzyl substitution, and nearly 20-fold (310 µM) with the vinylbenzyl and trifluoromethylbenzyl substitutions. This solubility enhancement suggests that the reported yields of the functionalized ZrMOPs were likely deflated due to the work-up method used. Collection of only the precipitate and washing with DMF, paired with an increased saturation limit, served to decrease yield.

Conclusions

We have established that ZrMOP node-functionalization is possible through synthetic chemistry, and that these functionalizations have ramifications on ZrMOP properties. Through the synthesis of functionalized cyclopentadienyl ligands, and corresponding functionalized zirconocene precursors, a series of ZrMOPs was synthesized with benzyl-, vinylbenzyl-, and trifluoromethylbenzyl-pendant groups decorating the cyclopentadienyl capping moieties. The ZrMOPs were isolated as tetrahedral architectures using the same self-assembly conditions as the unfunctionalized ZrMOP, and

with no decrease in yields, showing that the self-assembly process was not hindered by additional node-functionality.

The effects of node-functionalization were studied using inductively coupled plasma mass spectrometry. Most notably, there was a 20-fold enhancement of **ZrMOP-vb** and **ZrMOP-tfmb** solubility in dimethylformamide compared to **ZrMOP**. Additionally, a 7-fold decrease in water solubility was observed in all functionalized ZrMOPs. These results are significant because increasing organic solubility can enhance the processibility of ZrMOPs for use in materials applications. Decreasing water solubility can also be beneficial in atmospheric/aqueous applications, where these water stable ZrMOPs must remain incorporated in the material matrix.

In addition to showing how ZrMOP node-functionalization can be used to tune solubility, this work establishes ZrMOP nodes as accessible sites for functionalization that may be used to alter other physiochemical properties of ZrMOPs. With independent modification now accessible at both the bridging ligands and nodes, bifunctional ZrMOPs are more tunable than previously realized, and can be explored for unique reactivity and emergent properties.

Author Contributions

Meghan G. Sullivan conducted all experimental work, and contributed to conceptualization, investigation, data curation, formal analysis, visualization, and writing.
Gregory E. Sokolow contributed to conceptualization, data curation, formal analysis, and writing – review & editing.
Eric T. Jensen was responsible for data curation and formal analysis of high-resolution mass spectrometry data.
Matthew R. Crawley contributed to formal analysis of crystallographic data.
Samantha N. MacMillan was responsible for data curation of crystallographic data.
Timothy R. Cook provided conceptualization, project administration, resources, funding acquisition, supervision, and writing – review & editing.

Conflicts of interest

There are no conflicts to declare.

Acknowledgements

This work was supported by the Department of Energy (DEFE0031736). M.G.S. was supported by the NSF REU program (CHE-1852372), and a Peter T. Lansbury Scholarship sponsored by Joseph Vacca and awarded by the UB Department of Chemistry. Characterization was carried out using the UB CIC facilities, including the Bruker SolariXR FT-ICRMS (NIH S10 RR029517) and the ThermoElectron X Series 2 ICP-MS (NSF MRI CHE-0959565). Nuclear magnetic resonance experiments were carried out in the UB MR Center using the Bruker AVANCE NEO 500 MHz NMR (NSF CHE-2018160).

References

1. T. R. Cook and P. J. Stang, *Chem. Rev.*, 2015, **115**, 7001-7045.
2. T. R. Cook, Y.-R. Zheng and P. J. Stang, *Chem. Rev.*, 2013, **113**, 734-777.
3. A. J. Gosselin, C. A. Rowland and E. D. Bloch, *Chem. Rev.*, 2020, **120**, 8987-9014.
4. S. S.-Y. Chui, S. M.-F. Lo, J. P. H. Charmant, A. G. Orpen and I. D. Williams, *Science*, 1999, **283**, 1148-1150.
5. M. Eddaoudi, J. Kim, J. B. Wachter, H. K. Chae, M. O'Keeffe and O. M. Yaghi, *Journal of the American Chemical Society*, 2001, **123**, 4368-4369.
6. G. Liu, Z. Ju, D. Yuan and M. Hong, *Inorg. Chem.*, 2013, **52**, 13815-13817.
7. J. H. Cavka, S. Jakobsen, U. Olsbye, N. Guillou, C. Lamberti, S. Bordiga and K. P. Lillerud, *Journal of the American Chemical Society*, 2008, **130**, 13850-13851.
8. V. J. Pastore and T. R. Cook, *Chemistry of Materials*, 2020, **32**, 3680-3700.
9. E. V. Perez, K. J. Balkus, J. P. Ferraris and I. H. Musselman, *J. Membr. Sci.*, 2014, **463**, 82-93.
10. J. Ma, Y. Ying, Q. Yang, Y. Ban, H. Huang, X. Guo, Y. Xiao, D. Liu, Y. Li, W. Yang and C. Zhong, *Chem. Commun.*, 2015, **51**, 4249-4251.
11. C. Zhao, N. Wang, L. Wang, S. Sheng, H. Fan, F. Yang, S. Ji, J.-R. Li and J. Yu, *AIChE Journal*, 2016, **62**, 3706-3716.
12. C. R. P. Fulong, J. Liu, V. J. Pastore, H. Lin and T. R. Cook, *Dalton Trans.*, 2018, **47**, 7905-7915.
13. J. Liu, W. Duan, J. Song, X. Guo, Z. Wang, X. Shi, J. Liang, J. Wang, P. Cheng, Y. Chen, M. J. Zaworotko and Z. Zhang, *Journal of the American Chemical Society*, 2019, **141**, 12064-12070.
14. J. A. Foster, R. M. Parker, A. M. Belenguer, N. Kishi, S. Sutton, C. Abell and J. R. Nitschke, *Journal of the American Chemical Society*, 2015, **137**, 9722-9729.
15. T. Ji, L. Xia, W. Zheng, G.-Q. Yin, T. Yue, X. Li, W. Zhang, X.-L. Zhao and H.-B. Yang, *Polym. Chem.*, 2019, **10**, 6116-6121.
16. C. M. Brown, D. J. Lundberg, J. R. Lamb, I. Kevlishvili, D. Kleinschmidt, Y. S. Alfaraj, H. J. Kulik, M. F. Ottaviani, N. J. Oldenhuis and J. A. Johnson, *Journal of the American Chemical Society*, 2022, **144**, 13276-13284.
17. X. Qi, R. Zhong, M. Chen, C. Sun, S. You, J. Gu, G. Shan, D. Cui, X. Wang and Z. Su, *ACS Catalysis*, 2021, **11**, 7241-7248.
18. E.-S. M. El-Sayed, Y. D. Yuan, D. Zhao and D. Yuan, *Acc. Chem. Res.*, 2022, **55**, 1546-1560.
19. P. Delgado, J. D. Martin-Romera, C. Perona, R. Vismara, S. Galli, C. R. Maldonado, F. J. Carmona, N. M. Padial and J. A. R. Navarro, *ACS Appl. Mater. Interfaces*, 2022, **14**, 26501-26506.
20. Y.-H. Zou, Q.-J. Wu, Q. Yin, Y.-B. Huang and R. Cao, *Inorg. Chem.*, 2021, **60**, 2112-2116.
21. W.-H. Xing, H.-Y. Li, X.-Y. Dong and S.-Q. Zang, *J. Mater. Chem. A*, 2018, **6**, 7724-7730.
22. Z. Xiao, H. F. Drake, Y. H. Rezenom, P. Cai and H.-C. Zhou, *Small Structures*, 2022, **3**, 2100133.
23. A. J. Gosselin, G. E. Decker, B. W. McNichols, J. E. Baumann, G. P. A. Yap, A. Sellinger and E. D. Bloch, *Chem. Mater.*, 2020, **32**, 5872-5878.
24. G. Liu, Y. Di Yuan, J. Wang, Y. Cheng, S. B. Peh, Y. Wang, Y. Qian, J. Dong, D. Yuan and D. Zhao, *J. Am. Chem. Soc.*, 2018, **140**, 6231-6234.

25. Y. Li, J. Dong, W. Gong, X. Tang, Y. Liu, Y. Cui and Y. Liu, *Journal of the American Chemical Society*, 2021, **143**, 20939-20951.
26. E. J. Palmer, R. J. Strittmatter, K. T. Thornley, J. C. Gallucci and B. E. Bursten, *Polyhedron*, 2013, **58**, 120-128.
27. J. T. Foy, E. B. Wilkes and I. Aprahamian, *CrystEngComm*, 2012, **14**, 6126-6128.
28. S. Hok, J. Vassilian and N. E. Schore, *Organic Letters*, 2002, **4**, 2365-2368.
29. H. G. Alt, C. E. Denner and W. Milius, *Inorganica Chimica Acta*, 2004, **357**, 1682-1694.
30. S. Chen, S. Cheng, L. Zhao, C. Sun, C. Qin and Z. Su, *New J. Chem.*, 2020, **44**, 21255-21260.
31. A. Martín-Cameán, A. Jos, A. Calleja, F. Gil, A. Iglesias, E. Solano and A. M. Cameán, *Talanta*, 2014, **118**, 238-244.
32. M. Yaman, M. Ince, E. Erel, E. Cengiz, T. Bal, C. Er and F. Kilicel, *CLEAN – Soil, Air, Water*, 2011, **39**, 530-536.
33. J. C. Stern, D. I. Foustoukos, J. E. Sonke and V. J. M. Salters, *Chem. Geol.*, 2014, **363**, 241-249.
34. C. Reichardt and T. Welton, in *Solvents and Solvent Effects in Organic Chemistry*, 2010, DOI: 10.1002/9783527632220.app1, pp. 549-586.